ELSEVIER

Predicting shock dynamics in the presence of uncertainties

G. Lin, C.-H. Su, G.E. Karniadakis *

Division of Applied Mathematics, Brown University, 182 George Street, Box F, Providence, RI 2912, United States

Abstract

We revisit the classical aerodynamics problem of supersonic flow past a wedge but subject to random inflow fluctuations or random wedge oscillations around its apex. We first obtain analytical solutions for the inviscid flow, and subsequently we perform stochastic simulations treating randomness both as a steady as well as a time-dependent process. We use a multi-element generalized polynomial chaos (ME-gPC) method to solve the two-dimensional stochastic Euler equations. A Galerkin projection is employed in the random space while WENO discretization is used in physical space. A key issue is the characteristic flux decomposition in the stochastic framework for which we propose different approaches. The results we present show that the variance of the location of perturbed shock grows quadratically with the distance from the wedge apex for steady randomness. However, for a time-dependent random process the dependence is quadratic only close to the apex and linear for larger distances. The multi-element version of polynomial chaos seems to be more effective and more efficient in stochastic simulations of supersonic flows compared to the global polynomial chaos method.
© 2006 Elsevier Inc. All rights reserved.

Keywords: Supersonic flow; Stochastic simulations; Polynomial chaos; Random inflow

1. Introduction

Studies of noisy supersonic flow past aerodynamic objects are very limited. On the experimental side, the presence of inherent noise in high-speed wind tunnels make them unreliable predictors of fight performance, except in special cases [1]. In flight conditions, the sources of such ''noise'' may be different; for example, random disturbances may arise due to turbulence or due to other local small-scale events such as microbursts. However, even at subsonic conditions in unsteady flows past bluff objects, small amounts of noise may have a potentially dramatic effect on the structure of the *mean* flow. This was demonstrated in [2] for a uniform but noisy flow past an oscillating circular cylinder. In the absence of any disturbances a vortex street is formed in the wake characterized by the shedding of three vortices per shedding cycle, the so-called (P + S) pattern [3]. However, when noise is introduced at the inflow the vortex street *switches* to another state above a certain noise threshold, characterized by only two vortices per shedding cycle, as in the standard von Karman street for stationary cylinders (2S pattern). This phenomenon is discussed in detail in [2] and independent experimental validation can be found in [4].

---

* Corresponding author. Tel.: +1 401 863 1217; fax: +1 401 863 3369.
  E-mail address: gk@dam.brown.edu (G.E. Karniadakis).

For supersonic flows, random inflow disturbances may also modify substantially the flow field rendering traditional predictive CFD tools invalid. We demonstrate here such global flow structure change with a deterministic example. We consider supersonic flow (Mach number 2) past a wedge of angle $\theta = 14.7°$ subject to a small time-dependent inflow variation superimposed on a uniform inflow. Specifically, the two-dimensional velocity field is given by

$$u = u_1 \cos \theta (1 + \epsilon \sin(\omega \pi t)), \quad v = -u_1 \sin \theta (1 + \epsilon \sin(\omega \pi t)), \tag{1}$$

where the notation, solution algorithms and a sketch of the set-up are explained in detail in the next two sections. Here, we plot the streamlines of the flow and the shock in Fig. 1 for $\epsilon = 0.06$ and $\omega = 1$. We see that both the streamlines and the shock are visibly perturbed with respect to the familiar classical "clean inflow" picture [5].

In this paper, we study the shock dynamics in two-dimensional supersonic flows past a wedge assuming two different random disturbances. These correspond to random inflow velocity or random oscillations of the wedge around its apex and they can be steady in-time or time-dependent. The latter could be a model for aeroelastic motions, e.g. for the flutter oscillations. Our goal is to develop robust predictive CFD tools to simulate these cases and evaluate these new tools. To this end, we will also develop analytical stochastic solutions for the wedge problem in the spirit of our previous work on the stochastic piston problem [6].

Specifically, we are interested in applying *polynomial chaos* to compressible flow problems. This method, first introduced by Ghanem and co-workers for various problems in mechanics [7,8], models uncertainty by a spectral expansion based on Hermite orthogonal polynomials in terms of Gaussian random variables. A broader representation but within the same Galerkin framework as in [7], called "generalized polynomial chaos", was introduced in [9,10]. This version employs a broad family orthogonal polynomials from the Askey scheme as the expansion basis to represent non-Gaussian processes more efficiently; it includes the classical Hermite polynomial chaos as a subset. This version can be thought of as a counterpart of the *global* spectral method applied in simple-geometry deterministic PDEs. We also study in the current work a multi-element version of generalized polynomial chaos, similar to spectral/hp element method, but decomposing the multi-dimensional *random space* in a non-conforming fashion.

The paper is organized as follows: In Section 2, we derive simple analytical stochastic solutions, and in Section 3, we present the numerical methodology. In Section 4, we present numerical results from stochastic simulations based on the aforementioned two versions of polynomial chaos but also on Monte-Carlo simulations. We conclude in Section 5 with a brief discussion. In Appendix A we give details of the Galerkin projection and the derived modified Euler equations obtained using generalized polynomial chaos (gPC) and multi-element generalized polynomial chaos (ME-gPC).
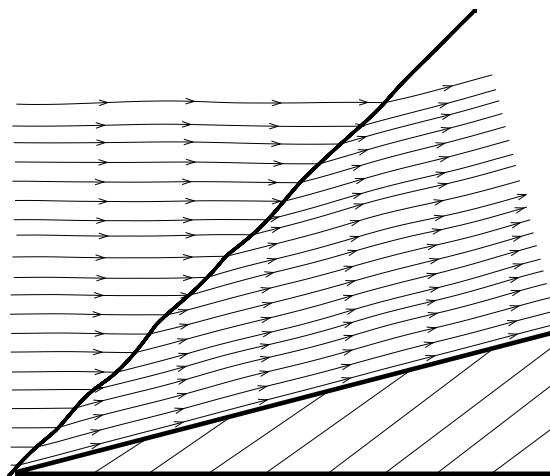
Fig. 1. Supersonic flow past a wedge: instantaneous streamlines and perturbed shock path induced by small time-dependent inflow perturbations at inflow Mach number $M_1 = 2$.

2. Stochastic analytical solutions

We consider the perturbation of an oblique attached shock in supersonic flow past a wedge due to time-varying random inflow or random wedge motions. A schematic of this problem is shown in Fig. 2. We consider small perturbations and we also assume that the perturbation of the shock slope is small. The flow between the shock and the wedge is approximated as isentropic.

We denote the wedge angle by θ, the shock angle by χ and the incoming flow velocity W_1 with its normal component $u_1 = W_1 \sin \chi$. The streamlines behind the shock are parallel to the wedge surface, and we denote the velocity by W_2 and its normal component to the shock by $u_2 = W_2 \sin(\chi - \theta) = W_1 \cos \chi \tan(\chi - \theta)$. Using the normal shock relations we have

$$\frac{P_2}{P_1} = 1 + \frac{2\gamma}{1 + \gamma}(M_1^2 \sin^2 \chi - 1), \tag{2a}$$

$$\frac{\rho_1}{\rho_2} = \frac{(\gamma - 1)M_1^2 \sin^2 \chi + 2}{(\gamma + 1)M_1^2 \sin^2 \chi}, \tag{2b}$$

$$\tan(\chi - \theta) = \tan \chi \frac{(\gamma - 1)M_1^2 \sin^2 \chi + 2}{(\gamma + 1)M_1^2 \sin^2 \chi} \equiv S(\chi), \tag{2c}$$

where the subscripts 1 and 2 correspond to the state going into and coming out of the shock, respectively. Also, $M_1 = \frac{W_1}{C_1}$ and $C_1^2 = \gamma \frac{P_1}{\rho_1}$. We use Eq. (2c) to solve for θ in terms of χ, thus

$$\tan \theta = 2 \cot \chi \frac{M_1^2 \sin^2 \chi - 1}{M_1^2(\gamma + \cos 2\chi) + 2} \tag{3a}$$

or

$$\theta = \chi - \tan^{-1}(S(M_1, \chi)). \tag{3b}$$

From Eq. (3a), the following cubic equation for $\tan \chi$ can be derived

$$\tan \theta [M_1^2(\gamma - 1) + 2] \tan^3 \chi + 2(1 - M_1^2) \tan^2 \chi + \tan \theta [M_1^2(\gamma + 1) + 2] \tan \chi + 2 = 0 \tag{4}$$

and we obtain three solutions by solving the above cubic equation. From oblique shock theory, for a given initial Mach number M_1, we have the following range of possible shock angles

$$\sin^{-1} \frac{1}{M_1} \leqslant \chi \leqslant \frac{\pi}{2}. \tag{5}$$
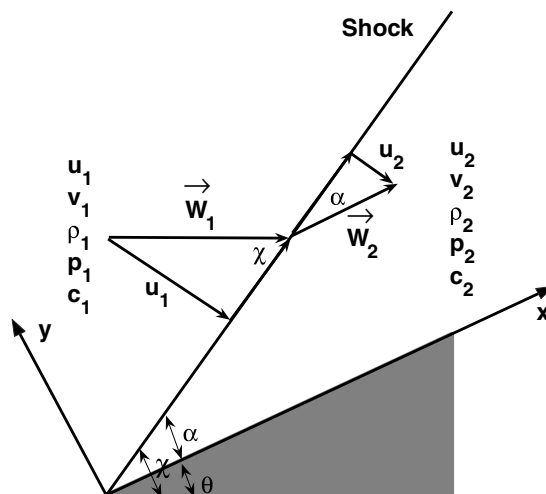
Fig. 2. Sketch of supersonic flow past a wedge and definition of coordinate system.

In the following, we will denote the unique shock angle χ obtained from Eqs. (4) and (5) as

$$\chi = R(\theta, M_1). \tag{6}$$

We now consider random perturbations at the inflow or for the wedge motion, both described as *uniform random variables* in the form:

$$M_1' = M_1(1 + \epsilon\xi), \quad u_w' = W_1\epsilon\xi, \tag{7}$$

where $\xi \in [-1,1]$ is a *uniform* random variable and ϵ is the amplitude of the perturbation. The perturbed shock path $z(x)$ is then

$$z(x, \xi) = x[\tan(R(\xi) - \theta_0) - \tan(\chi_0 - \theta_0)] \equiv xG(\xi), \tag{8}$$

where χ_0 is the unperturbed shock angle. The mean and variance of the perturbed shock path can be obtained as

$$\langle z(x, \xi)\rangle = \int_D z(x, \xi)f(\xi)\,\mathrm{d}\xi = x\int_D G(\xi)f(\xi)\,\mathrm{d}\xi, \tag{9a}$$

$$\mathrm{Var}(z(x, \xi)) = \int_D z^2(x, \xi)f(\xi)\,\mathrm{d}\xi - \left(\int_D z(x, \xi)f(\xi)\,\mathrm{d}\xi\right)^2 = x^2\left(\int_D G^2(\xi)f(\xi)\,\mathrm{d}\xi - \left(\int_D G(\xi)f(\xi)\,\mathrm{d}\xi\right)^2\right), \tag{9b}$$

where $f(\xi)$ is the PDF of the random variable ξ. From Eq. (9a) we can see that the mean of the perturbed shock path is proportional to x while from Eq. (9b) we see that the corresponding variance is proportional to x^2. Since Eq. (8) is derived directly from the Rankine–Hugoniot relations (Eqs. (2a)–(2c)), it implies that Eq. (8) is still valid even for large random perturbation as long as the shock is attached to the wedge. However, if the perturbation of the random inflow is small we can use appropriate approximations to derive simple analytical expressions for the mean and variance of the perturbed shock. The following expressions can be derived from Eqs. (3a) and (3b):

$$\frac{\mathrm{d}M_1}{\mathrm{d}\chi} = \frac{M_1^2\sin^2\chi(\cos 2\chi + \tan\theta\sin 2\chi) + 1}{M_1\sin^2\chi[\tan\theta(\gamma + \cos 2\chi) - \sin 2\chi]} \equiv H(M_1, \chi, \theta). \tag{10}$$

Next, we derive simpler expressions for cases with small random perturbations.

2.1. Small random inflow perturbations

First, let us assume that the wedge angle is fixed but the shock is under random inflow perturbation described as a uniform *random variable* as shown in Eq. (7). We have

$$z(x, \xi) = x\left[\tan\left(\chi_0 - \theta_0 + \frac{\Delta M_1}{H(\chi)}\right) - \tan(\chi_0 - \theta_0)\right] = x(1 + s^2)\frac{\Delta M_1}{H(\chi)}, \tag{11}$$

where $s = \tan(\chi_0 - \theta_0)$ and ΔM_1 is the perturbed part of the inflow Mach number. The mean and variance of the perturbed shock path are then

$$\langle z(x, \xi)\rangle = 0, \quad \mathrm{Var}(z(x, \xi)) = x^2(1 + s^2)^2\frac{M_1^2\epsilon^2\langle\xi^2\rangle}{H^2(\chi)} = x^2(1 + s^2)^2\frac{M_1^2\epsilon^2}{3H^2(\chi)}. \tag{12}$$

From Eq. (12) we see that when the random inflow is described as a uniform random variable with small amplitude ϵ, the mean of the perturbed shock path is zero while the variance scales quadratically with the distance from the wedge apex.

2.2. Small random wedge oscillations

Next, we assume that the wedge inflow is deterministic but the wedge oscillations are described as a uniform random variable, as shown in Eq. (7). In this case we obtain

$$z(x, \xi) = x\left[\tan\left(\chi_0 - \theta_0 - \frac{M_1\epsilon\xi}{H(\chi)}\right) - \tan(\chi_0 - \theta_0)\right] = -x(1 + s^2)\frac{M_1\epsilon\xi}{H(\chi)}. \tag{13}$$

The mean and variance of the perturbed shock path are

$$\langle z(x, \xi)\rangle = 0, \quad \mathrm{Var}(z(x, \xi)) = x^2(1 + s^2)^2\frac{M_1^2\epsilon^2\langle\xi^2\rangle}{H^2(\chi)} = x^2(1 + s^2)^2\frac{M_1^2\epsilon^2}{3H^2(\chi)}. \tag{14}$$

The mean and variance for this case are similar to the previous case, consistent with physical intuition.

3. Numerical methods

We solve the two-dimensional Euler equations for supersonic flow past a wedge for the two aforementioned cases: (1) random inflow, and (2) random wedge oscillations. In the latter case, we employ a transformation based on a boundary-fitted coordinate system approach so that we solve the Euler equations in a stationary domain. In order to compare differences with the analytical solutions we will perform two types of stochastic simulations following a Monte-Carlo approach and a polynomial chaos approach.

3.1. Transformed Euler equations

We consider the two-dimensional Euler equations

$$\begin{aligned}
&\frac{\partial\rho}{\partial t} + \frac{\partial\rho u}{\partial x} + \frac{\partial\rho v}{\partial y} = 0, \\
&\frac{\partial\rho u}{\partial t} + \frac{\partial}{\partial x}(\rho u^2 + p) + \frac{\partial}{\partial y}(\rho uv) = 0, \\
&\frac{\partial\rho v}{\partial t} + \frac{\partial}{\partial x}(\rho uv) + \frac{\partial}{\partial y}(\rho v^2 + p) = 0, \\
&\frac{\partial E}{\partial t} + \frac{\partial}{\partial x}[u(p + E)] + \frac{\partial}{\partial y}[v(p + E)] = 0,
\end{aligned} \tag{15}$$

where ρ denotes density, u and v are x and y component velocity, E is total energy, $m = \rho u$ and $n = \rho v$ are the x and y component momentum, and γ is the ratio of the specific heats. Also, p is the pressure with $p = (\gamma - 1)(E - \frac{1}{2}\rho(u^2 + v^2))$. All flow quantities, i.e., pressure, x and y velocity components as well as momentum and total energy are treated as stochastic processes. A random dimension, denoted by the parameter ξ, is introduced in addition to the spatial–temporal dimensions (x, y, t), thus

$$u = u(x, y, t; \xi), \quad v(x, y, t; \xi), \quad p = p(x, y, t; \xi), \quad m = m(x, y, t; \xi), \quad E = E(x, y, t; \xi). \tag{16}$$

To deal with the moving boundaries of the wedge, we adopt a boundary-fitted coordinate approach. By attaching the coordinate system to the wedge, the wedge appears stationary in time with respect to the new coordinate system. Specifically, we define two coordinate systems (x, y, t) and (ζ, η, τ), where (x, y, t) is the original coordinate system and (ζ, η, τ) is the transformed one. The mapping between the two systems is:

$$\begin{aligned}
&\zeta = x - \int_0^\tau u_\mathrm{w}(\tau_1, \xi)\cos\theta\,\mathrm{d}\tau_1, \\
&\eta = y + \int_0^\tau u_\mathrm{w}(\tau_1, \xi)\sin\theta\,\mathrm{d}\tau_1, \\
&\tau = t,
\end{aligned} \tag{17}$$

where u_w is the stochastic wedge motion in inflow direction and θ is the wedge angle. This mapping simply reduces to the new velocities u_r, v_r being shifted by the reference frame velocity, i.e.,

$$\begin{aligned}
&u_\mathrm{r} = u - u_\mathrm{w}(t, \xi)\cos\theta, \\
&v_\mathrm{r} = v + u_\mathrm{w}(t, \xi)\sin\theta.
\end{aligned} \tag{18}$$

It is worth noting that this mapping is stochastic when the wedge motion is random and needs to be represented by the chaos expansion as well. The compressible Euler equations (15) with stochastic time-dependent boundary conditions are transformed into:

$$
\begin{aligned}
&\frac{\partial \rho}{\partial \tau} + \frac{\partial \rho u_r}{\partial \zeta} + \frac{\partial \rho v_r}{\partial \eta} = 0, \\
&\frac{\partial \rho u_r}{\partial \tau} + \frac{\partial}{\partial \zeta}(\rho u_r^2 + p) + \frac{\partial}{\partial \eta}(\rho u_r v_r) = -\rho \cos\theta \frac{\partial u_w}{\partial \tau}, \\
&\frac{\partial \rho v_r}{\partial \tau} + \frac{\partial}{\partial \zeta}(\rho u_r v_r) + \frac{\partial}{\partial \eta}(\rho v_r^2 + p) = \rho \sin\theta \frac{\partial u_w}{\partial \tau}, \\
&\frac{\partial E_r}{\partial \tau} + \frac{\partial}{\partial \zeta}[u_r(p + E_r)] + \frac{\partial}{\partial \eta}[v_r(p + E_r)] = \rho \frac{\partial u_w}{\partial \tau}(v_r \sin\theta - u_r \cos\theta),
\end{aligned}
\tag{19}
$$

where $E_r = \frac{p}{\gamma-1} + \frac{1}{2}\rho(u_r^2 + v_r^2)$.

We model the wedge motion as a process

$$
u_w = W_1 + v_w = W_1(1 + \epsilon V(t, \xi)),
\tag{20}
$$

where v_w is perturbation component of the wedge motion. In the boundary-fitted coordinate system the stochastic moving wedge problem becomes similar to the stationary stochastic inflow wedge problem. The stochastic inflow can be expressed as

$$
\begin{aligned}
u_r &= u - W_1(1 + \epsilon V(t, \xi))\cos\theta, \\
v_r &= v + W_1(1 + \epsilon V(t, \xi))\sin\theta.
\end{aligned}
\tag{21}
$$

Specifically, we consider different representations of the stochastic inputs $V(t, \xi)$ corresponding to a random process with zero mean and exponential covariance, i.e.,

$$
\begin{aligned}
&\langle V(t, \xi) \rangle = 0, \\
&\langle V(t_1, \xi), V(t_2, \xi) \rangle = e^{-\frac{|t_1 - t_2|}{A}}.
\end{aligned}
\tag{22}
$$

A corresponding first-order Markov chain is employed to represent discretely the exponential kernel as follows:

$$
\begin{aligned}
V_0 &= \xi_0, \\
V_1 &= bV_0 + f\xi_1, \\
&\cdots \\
V_{i+1} &= bV_i + f\xi_{i+1},
\end{aligned}
$$

where $b = e^{\frac{-\Delta t}{A}}$ and $f = \sqrt{1 - b^2}$. In the Monte-Carlo simulation, a random wedge velocity $u_w = U_w(1 + \epsilon V_i(t, \xi))$ is selected from the above Markov chain as a stochastic input at each time step t_i. In the polynomial chaos representation we employ the Wiener–Legendre expansions (see next subsection) for all conservative and derived stochastic variables. The representation of *stochastic inputs* is accomplished by a Karhunen–Loeve decomposition [7].

We solve the Euler equations based on the coordinate system attached to the wedge. We then have to transform the solutions back to the original coordinate system:

$$
\begin{aligned}
x &= \zeta + \int_0^\tau u_w(\tau_1, \xi)\, d\tau_1, \\
y &= \eta, \\
t &= \tau,
\end{aligned}
\tag{23}
$$

where x and ζ denote the x-coordinate in the original coordinate system and in the transformed coordinate system, respectively. The shock location y includes the static part and the perturbed part. The perturbed shock location is defined as $z(\tau) = y - x\tan\alpha$.

The mean and variance of the perturbed shock paths are obtained numerically from:

$$\bar{z}(\tau) = \frac{1}{n} \sum_{i=0}^{n} z_i(\tau),$$

$$\langle z^2(\tau) \rangle = \frac{1}{n-1} \sum_{i=0}^{n} (z_i(\tau) - \bar{z}(\tau))^2,$$

(24)

where n is the total number of samples in the Monte-Carlo simulation.

3.2. Characteristic decomposition of the stochastic flux

In this section, we illustrate some of the difficulties associated with the nonlinear terms in the stochastic Euler equations and propose different approaches. Let us consider the one-dimensional system

$$u_t + f(u)_x = 0,$$

(25a)

written in non-conservative form

$$u_t + Au_x = 0,$$

(25b)

where $A(u) = \frac{\partial f}{\partial u}$. In the deterministic framework we can decompose the Jacobian matrix A into its characteristic form to obtain a diagonal matrix of eigenvalues D, that is

$$L \cdot A \cdot R = D \Rightarrow A = R \cdot D \cdot L,$$

(26)

where L and R are the left and right eigenvectors of A and $R \cdot L = I$. However, in the stochastic framework it is not so obvious how to obtain the characteristic form and if it exists. Let us employ the gPC expansion (see next subsection, also [9])

$$u = \sum_{i=0}^{N_p} \hat{u}_i \phi_i, \quad A = \sum_{i=0}^{N_p} \widehat{A}_i \phi_i,$$

(27)

where N_p is the total number of basis modes. From Eq. (25b), we have

$$\frac{\partial \hat{u}_k}{\partial t} + A' \cdot \left\{ \frac{\partial \hat{u}_j}{\partial x} \right\} = 0,$$

(28)

where

$$A' = \{a'_{k,j}\} = \left\{ \frac{\sum_{i=0}^{N_p} \widehat{A}_i e_{i,j,k}}{e_{0,k,k}} \right\}.$$

(29)

Here $e_{i,j,k} = \langle \phi_i \phi_j \phi_k \rangle$, $e_{0,k,k} = \langle \phi_k^2 \rangle$ and A' is a $(d+2)(N_p+1) \times (d+2)(N_p+1)$ matrix (d is the number of spatial dimensions).

We can decompose the Jacobian matrix A' into its characteristic form to obtain a diagonal matrix of eigenvalues D', that is,

$$L' \cdot A' \cdot R' = D' \Rightarrow A' = R' \cdot D' \cdot L',$$

(30)

where L' and R' are the left and right eigenvectors of A' and $R' \cdot L' = I$. Eq. (28) can be rewritten as

$$\frac{\partial \hat{u}_k}{\partial t} + R' \cdot D' \cdot L' \cdot \left\{ \frac{\partial \hat{u}_j}{\partial x} \right\} = 0.$$

(31)

By linearizing Eq. (31) around the Roe-average state and treat the eigenvector matrices as constant, we obtain

$$R'^{-1} \cdot \frac{\partial \hat{u}_k}{\partial t} + D' \cdot L' \cdot \left\{ \frac{\partial \hat{u}_j}{\partial x} \right\} = L' \cdot \frac{\partial \hat{u}_k}{\partial t} + D' \cdot L' \cdot \left\{ \frac{\partial \hat{u}_j}{\partial x} \right\} = 0.$$

(32)

This system is a decoupled system in terms of the characteristic variables $L' \cdot \hat{u}_k$. Therefore, we are able to apply upwinding techniques or Riemann solvers as in the standard deterministic CFD formulation [11].

In this paper, we employ the fifth-order WENO scheme in spatial discretization and a third-order Runge–Kutta method in time, see details in [12]. In the WENO scheme the sign of the eigenvalues is required in order to choose the proper stencils for differentiation in physical space. In the stochastic framework, we assume $f(u, \xi) = \sum_{i=0}^{N_p} \hat{f}_i \phi_i$, and thus Eq. (25a) can be written as

$$\sum_{i=0}^{N_p} \frac{\partial \hat{u}_i}{\partial t} \phi_i + \sum_{i=0}^{N_p} \frac{\partial \hat{f}_i}{\partial x} \phi_i = 0. \tag{33}$$

By projecting with ϕ_i for each $i \in [0, N_p]$ and employing the orthogonality relation, we obtain for each $i \in [0, N_p]$

$$\frac{\partial \hat{u}_i}{\partial t} + \frac{\partial \hat{f}_i}{\partial x} = \frac{\partial \hat{u}_i}{\partial t} + \frac{\langle f_x \phi_i \rangle}{\langle \phi_i^2 \rangle} = 0. \tag{34}$$

Using this approach, the characteristic flux decomposition technique of the deterministic framework can be used here to construct the numerical flux. However, it requires to compute $\langle f_x \phi_i \rangle = \int_D f_x \phi_i F(\xi) \, d\xi$ at each step, where $F(\xi)$ is the PDF of the random variables ξ. This approach will become computational expensive, especially as the stochastic dimension is increasing.

In order to enhance the computational efficiency of the stochastic solver, we can use the *mean* of the left and right eigenvectors, $\overline{L}$ and $\overline{R}$ from Eq. (26) to approximate the left and right eigenvectors in the stochastic framework. Since $\overline{L}$ and $\overline{R}$ are only used to choose the stencils, the approximation error of using the mean of the left and right eigenvectors will not affect the numerical results significantly, at least for relatively small amplitudes of the random perturbation. Another choice is to use *random* left and right eigenvectors at each time step evaluated at some value ξ_i. In the next section, we will show comparison of the aforementioned approaches.

Finally, an alternative approach is to employ a collocation projection by considering the nodal expansions

$$u(x, t, \xi) = \sum_{j=0}^{\kappa} u(x, t, p_j) L_j(\xi), \quad f(x, t, \xi) = \sum_{j=0}^{\kappa} f(x, t, p_j) L_j(\xi), \tag{35}$$

where $\{p_j\}$ are $(\kappa + 1)$ d-dimensional random points and $\{L_j(\xi)\}$ are Lagrangian interpolants, i.e., $L_j(p_i) = \delta_{i,j}$. This leads to an uncoupled system,

$$\frac{\partial u_\kappa(x, t, p_j)}{\partial t} + \frac{\partial f_\kappa(x, t, p_j)}{\partial x} = 0, \tag{36}$$

where $\{p_j\}$ is chosen from $(\kappa + 1)$ Gauss quadrature points. We then apply the characteristic flux decomposition technique in the deterministic framework to construct the numerical flux. Any deterministic numerical solver can be used to solve Eq. (36) for each Gauss quadrature point p_j in random space. We can construct the Lagrangian interpolant by Eq. (35) based on the $(\kappa + 1)$ Gauss quadrature points computed from Eq. (36). The mean and variance can be obtained from

$$\langle u \rangle = \sum_{j=0}^{\kappa} u(x, t, p_j) \int_D L_j(\xi) F(\xi) \, d\xi, \tag{37a}$$

$$\mathrm{Var}(u) = \int_D \left\{ \sum_{j=0}^{\kappa} u(x, t, p_j) L_j(\xi) \right\}^2 F(\xi) \, d\xi - \langle u \rangle^2. \tag{37b}$$

The collocation projection is easier to implement for nonlinear terms, as in the case of spectral methods for deterministic problems [13].

3.3. Multi-element generalized polynomial chaos (ME-gPC)

Polynomial chaos represents a stochastic process by a spectral expansion based on Hermite orthogonal polynomials in terms of Gaussian random variables. Its use in solving stochastic differential equations was pioneered by Ghanem and Spanos [7] who employed a Galerkin projection to derive an equivalent system

of deterministic equations; this can, typically, be solved with standard numerical techniques. A more recent version, generalized polynomial chaos (gPC), was proposed in [10] and employs a broader family of trial bases based on the orthogonal polynomials from the Askey scheme. We provide here a short overview of gPC and we also present a new more robust implementation based on decomposition of the random space into subregions. A general second-order random process $T(\xi(\theta))$ can be expressed by gPC as

$$T(x, y, t, \theta) = \sum_{i=0}^{N_p} \hat{T}_i(x, y, t) \phi_i(\xi_i(\theta)), \tag{38}$$

where the family $\{\phi_i\}$ is an orthogonal basis with orthogonality relation

$$\langle \phi_i, \phi_j \rangle = \langle \phi_i^2 \rangle \delta_{ij},$$

where δ_{ij} is the Kronecker delta, and $\langle \cdot, \cdot \rangle$ denotes the ensemble average. Here the ensemble average can be defined as the inner product in the Hilbert space in terms of the random vector $\xi = (\xi_1, \xi_2, \ldots, \xi_d)$, i.e.,

$$\langle f(\xi), g(\xi) \rangle = \int f(\xi) g(\xi) w(\xi) \, d\xi$$

or

$$\langle f(\xi), g(\xi) \rangle = \sum_{\xi} f(\xi) g(\xi) w(\xi)$$

in the discrete case, where $w(\xi)$ denotes the weight function. For a certain random vector ξ, the gPC basis $\{\phi_i\}$ can be chosen in such a way that its weight function has the *same form* as the probability distribution function of ξ. The total number of basis modes N_p is determined by the dimensionality of the chaos expansion d and the highest order p of the polynomials ϕ_i, where

$$N_p = \frac{(d+p)!}{(d!p!)} - 1. \tag{39}$$

An important aspect of the above chaos expansion is that the random processes are decomposed into a set of deterministic functions in the spatiotemporal variables multiplied by the random basis polynomials, which are independent of these variables.

The *multi-element generalized polynomial chaos* (ME-gPC) was proposed in [14] and decomposes the random space into elements within which gPC expansions are employed. Next, we summarize the theory developed in [14] but for *uniform distributions* only which we consider in the current work. For arbitrary distributions, the reader is referred to [15].

Let us take $\xi = (\xi_1, \xi_2, \ldots, \xi_d)$ to be a d-dimensional random vector and $\mathscr{P}(\Omega_i, \mathscr{A}_i, P_i)$ be the probability space of ξ_i. We assume that ξ_i are *uniform* random variables defined as $\xi_i : \Omega_i \mapsto [-1, 1]$ with a constant PDF $f_i = \frac{1}{2}$. Thus, ξ is a random vector defined as $\xi \mapsto B$ with a constant PDF $f = (\frac{1}{2})^d$, where $B = [-1,1]^d$.

B can be decomposed into a set $\mathbf{D}$ with N non-overlapping elements

$$\mathbf{D} = \begin{cases} B_k = [a_{k,1}, b_{k,1}] \times [a_{k,2}, b_{k,2}] \times \cdots \times [a_{k,d}, b_{k,d}], \\ B = \bigcup_k^N B_k, \\ B_{k_1} \bigcap B_{k_2} = \emptyset \quad \text{if } k_1 \neq k_2, \end{cases} \tag{40}$$

where $k, k_1, k_2 = 1, 2, \ldots, N$. In each element, a new d-dimensional *uniform* random vector is defined to be

$$\xi_k = g_k(\xi) = (\xi_{k,1}, \xi_{k,2}, \ldots, \xi_{k,d}) : \Omega_k \mapsto [-1, 1]^d \tag{41}$$

with a constant PDF $f^k = (\frac{1}{2})^d$. The new d-dimensional random vector can be mapped from a uniform random vector as following,

$$g_k(\xi) : \xi_i = \frac{b_{k,i} - a_{k,i}}{2} \xi_{k,i} + \frac{b_{k,i} + a_{k,i}}{2}, \quad i = 1, 2, \ldots, d. \tag{42}$$

The determinant of the Jacobian is the ratio of the volume of element k over the volume of the whole random space

$$\det\left|\frac{\partial\xi}{\partial\xi_k}\right| = \prod_{i=1}^{d}\frac{b_{k,i} - a_{k,i}}{2}. \tag{43}$$

In each element k, we implement gPC and solve the system according to ξ_k. The Karhunen–Loeve (K–L) decomposition for each element k can be expressed as:

$$u(\mathbf{t};\xi_k) = \overline{u}(\mathbf{t}) + \sum_{i=1}^{d}\sqrt{\lambda_i}f_i(\mathbf{t})\left(\frac{b_{k,i} - a_{k,i}}{2}\xi_{k,i} + \frac{b_{k,i} + a_{k,i}}{2}\right). \tag{44}$$

After we obtain the approximation $\hat{u}_k(\xi_k)$ for each element k ($k = 1,2,\ldots,N$), we can reconstruct the mth moment of $u(\xi)$ on the entire random domain,

$$\mu_m(u(\xi)) = \int_B u^m(\xi)\left(\frac{1}{2}\right)^d \mathrm{d}\xi = \sum_{k=1}^{N}\int_{[-1,1]^d}\hat{u}_k^m(\xi_k)\left(\frac{1}{2}\right)^d \det\left|\frac{\partial\xi}{\partial\xi_k}\right| \mathrm{d}\xi_k. \tag{45}$$

Let us assume that a general second-order random process u can be expressed by gPC expansion at random space in each element k:

$$u_k(\xi_k) = \sum_{j=0}^{N_p}\hat{u}_{k,j}\phi(\xi_j), \tag{46}$$

where p is the highest order of polynomial chaos and the total number of basis modes N_p is given in Eq. (39).

The *local mean* $\overline{u}_{k,p}$ and *local variance* $\sigma_{k,p}^2$ can be easily obtained from the orthogonality of gPC with order p

$$\overline{u}_{k,p} = \hat{u}_{k,0},$$
$$\sigma_{k,p}^2 = \sum_{j=1}^{N_p}\hat{u}_{k,j}^2\langle\phi_j^2\rangle. \tag{47}$$

The *global mean* $\overline{u}$ and the *global variance* σ^2 can be expressed as

$$\overline{u} = \sum_{k=1}^{N}\hat{u}_{k,0}\det\left|\frac{\partial\xi}{\partial\xi_k}\right|,$$
$$\sigma^2 = \sum_{k=1}^{N}\left[\sigma_{k,p}^2 + (\hat{u}_{k,0} - \overline{u})^2\right]\det\left|\frac{\partial\xi}{\partial\xi_k}\right|. \tag{48}$$

In Appendix A we give details of the Galerkin projection and the derived modified Euler equations obtained using gPC and ME-gPC.

4. Stochastic simulations

We now present representative results for the following conditions with respect to the boundary-fitted coordinate, as shown in Fig. 2. The length of the wedge is 5 while the angle of the shock is $\chi = 45°$, the angle of the wedge is $\theta = 14.7436°$, and the angle between the shock and the wedge is $\alpha = 30.2564°$. The inflow Mach number $M_1 = 2$, the inflow x velocity component is $u_1 = 1.9342$ and the y velocity component is $v_1 = -0.509$. Also, the sound speed is $C_1 = 1$, the pressure $p_1 = 1$, and the density $\rho_1 = 1.4$. On the outflow, the Mach number is $M_2 = 1.4563$, the x velocity component is $u_2 = 1.6372$ and the y velocity component is $v_2 = 0.0$. Finally, the sound speed is $C_2 = 1.2423$, the pressure $p_2 = 2.1667$ and the density $\rho_2 = 2.4$. We employ a fifth-order WENO scheme for spatial discretization with 150×150 grid points in the domain $[0,5] \times [0,5]$.

We provide all these quantities in detail so that the interested reader should be able to repeat our numerical experiments.

4.1. Random inflow

First, we consider the case where the inflow velocity is perturbed by random fluctuation described as a random variable with amplitude $\epsilon = 0.01$ and $\epsilon = 0.18$.

In order to quantify the differences in the various strategies we have developed for the characteristic decomposition of the flux term, we compare the different approaches in Fig. 3. In particular, we present the variance of the perturbed shock path for the larger amplitude value corresponding to three different decompositions, as detailed in the previous section. They correspond to employing (1) the mean values of L and R, (2) L and R evaluated at a random but specific point, and (3) the full projection described by Eq. (34). We see that all three approaches lead to good agreement with the available analytical solution even for the relatively large perturbation corresponding to $\epsilon = 0.18$. Therefore, at least for the current problem it appears that the specific characteristic treatment of the stochastic flux term does not affect the results; we expect that the collocation projection will also lead to the same result. As we stated earlier, within the WENO discretization that we employ in the current work, this decomposition provides the eigenvalues, the sign of which determines the differentiation stencils to be employed. Even if a different stencil is chosen at different grid points this will not affect the results visibly. On the other hand, the characteristic decomposition also determines how the boundary conditions are imposed. In the current supersonic inflow/outflow problem of inviscid dynamics there is no complication with the boundary conditions. However, in other problems with mixed conditions at the inflow or outflow, e.g. in viscous supersonic boundary layers, we expect the characteristic treatment of the stochastic flux to have a more pronounced effect.

Now we examine other flow features of interest and compare the polynomial chaos results against analytical results and Monte-Carlo simulations, first for a random variable case and subsequently for a random process case. In Fig. 4, we present the mean and variance of $\rho(\xi, x, y, t)$ corresponding to inflow perturbation described as a random variable with amplitude $\epsilon = 0.18$. We note that both quantities resemble a fan expansion. In Fig. 5, we plot the variance of the perturbed shock path as a function of the distance from the wedge apex x on the wedge surface for two amplitude values: $\epsilon = 0.01$ and $\epsilon = 0.18$. From Eq. (9b), we know that the variance of the perturbed shock is proportional to x^2. Indeed, for amplitude $\epsilon = 0.01$ we can verify that the perturbation solution from Eq. (12) and the analytical solution from Eq. (9b) match exactly. However, for amplitude $\epsilon = 0.18$ we see in Fig. 5 that the perturbation solution from Eq. (12) deviates from the analytical solution from Eq. (9b). This is expected, as for large amplitude, Eq. (12) does not hold and thus we have to employ Eq. (9b) to obtain the analytical solution. With respect
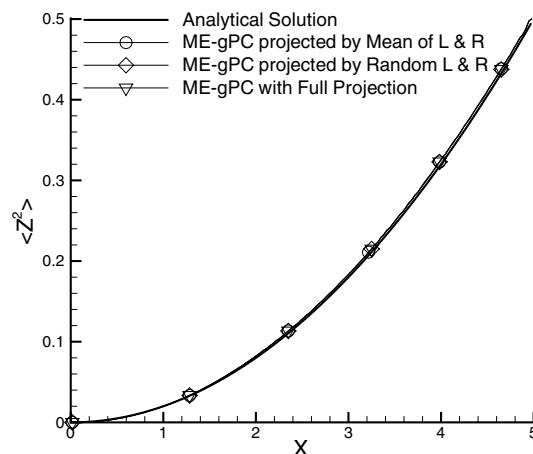
Fig. 3. Variance of the perturbed shock path as a function of the distance from the wedge apex x along the wedge surface. The random inflow perturbation is described as a random variable with amplitude, $\epsilon = 0.18$. The results are obtained from ME-gPC with full projection, based on the mean values of L and R, and based on values L and R obtained at random points.
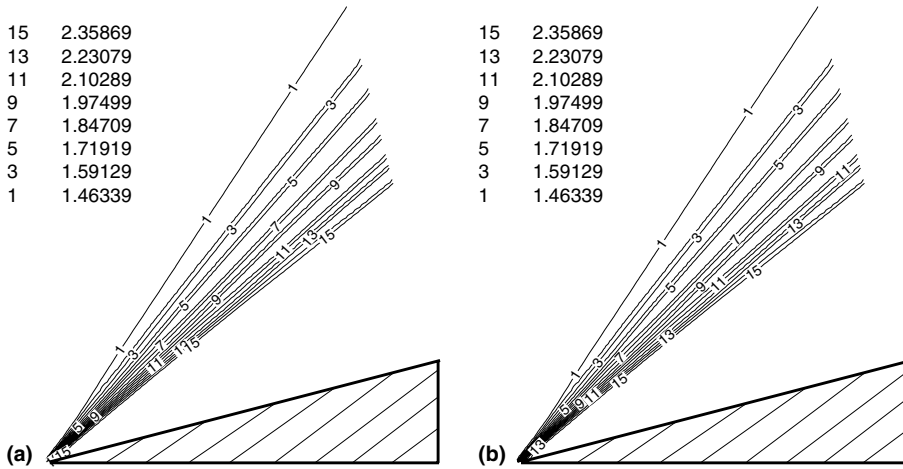
Fig. 4. Mean (a) and variance (b) of $\rho(\xi, x, y, t)$ induced by random inflow perturbation described as a random variable with amplitude, $\epsilon = 0.18$.
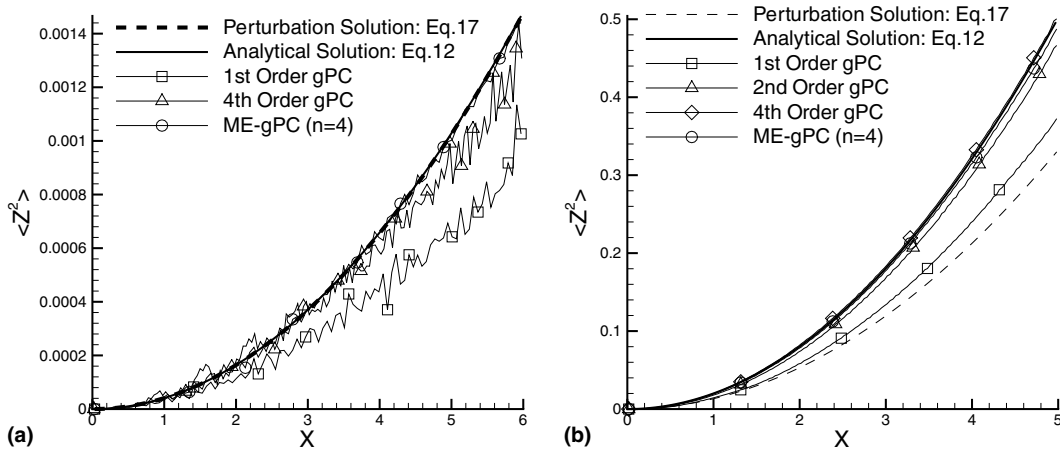
Fig. 5. Variance of the perturbed shock paths as a function of x induced by random inflow perturbation described as a random variable with amplitude: (a) $\epsilon = 0.01$ and (b) $\epsilon = 0.18$.

to the numerical solutions, we note that by increasing the (Legendre) polynomial order of gPC from $p = 1$ to $p = 4$ we achieve good agreement for both amplitudes. Decomposing the random space and using ME-gPC by employing $N = 4$ elements of first-order we also achieve very good agreement with the analytical solution. We have also performed convergence studies for this problem ($\epsilon = 0.18$) and we verified that in the ME-gPC method both mean and variance converge at a rate $N^{-2(p+1)}$, in agreement with estimates obtained in [16] but for stochastic elliptic problems.

We now consider a time-dependent random inflow perturbation described as a *random process* with zero mean and exponential covariance, see Eq. (22). As the value of the correlation time A increases we recover the random variable case corresponding to a fully-correlated (in-time) perturbation. On the other hand, the smaller the value of the correlation time A is the closer the perturbation resembles white noise. Here we will perform simulations for an intermediate value of correlation time $A = 1$. We will represent the random inflow process via a Karhunen–Loeve expansion with four modes. At this truncation the fifth eigenvalue is 36% percent of the first eigenvalue; here we neglect the effect of smaller scales for computational expedience.
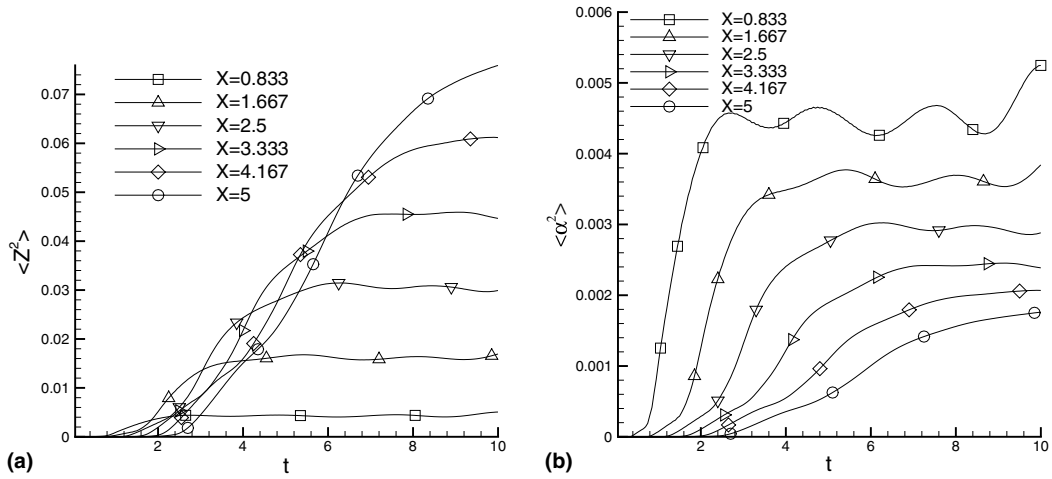
Fig. 6. Variance of (a) the perturbed shock path and (b) of the perturbed shock angle as a function of time t, induced by random time-dependent inflow perturbation described as a *random process* with correlation length $A = 1$ and amplitude $\epsilon = 0.1$.

Stochastic inputs characterized as random processes are significantly more difficult to simulate with polynomial chaos methods than inputs characterized as random variables. In the former case, we do not have analytical solutions available so we will compare the gPC and ME-gPC solutions against Monte-Carlo simulations.

In Fig. 6, we plot the variance of the perturbed shock path (left) and the variance of the perturbed shock angle (right) as a function of time t at different x locations for amplitude $\epsilon = 0.1$. In Fig. 7, we plot the same quantities but as a function of the distance from the wedge apex on the wedge surface at fixed time $t = 10$. We also compare the results against Monte-Carlo simulations obtained with 4000 samples and using the Karhunen–Loeve expansion to represent the stochastic inflow process. We see that in this case ME-gPC with $N = 16$ and 64 random elements give better results than the second-order gPC results; the latter deviate from the Monte-Carlo simulations at large x. This is because the variance of the perturbed shock is increasing as x increases and thus high-order gPC expansions are required to simulate this problem with large variance. We have also performed similar simulations but for amplitude $\epsilon = 0.01$ (results not shown here) and the agreement between ME-gPC with Monte-Carlo simulation is even better.
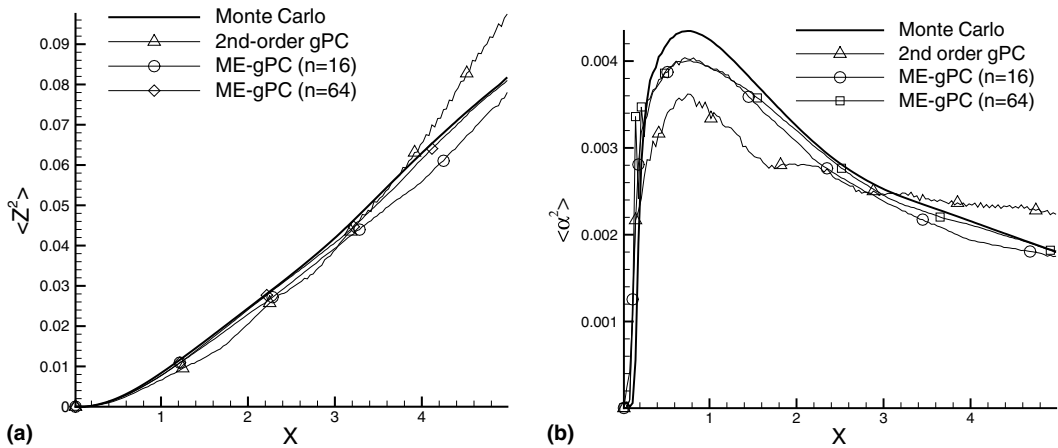
Fig. 7. Variance of (a) the perturbed shock path and (b) of the perturbed shock angle as a function of distance x at $t = 10$, induced by random time-dependent inflow perturbation described as a *random process* with correlation length $A = 1$ and amplitude $\epsilon = 0.1$.
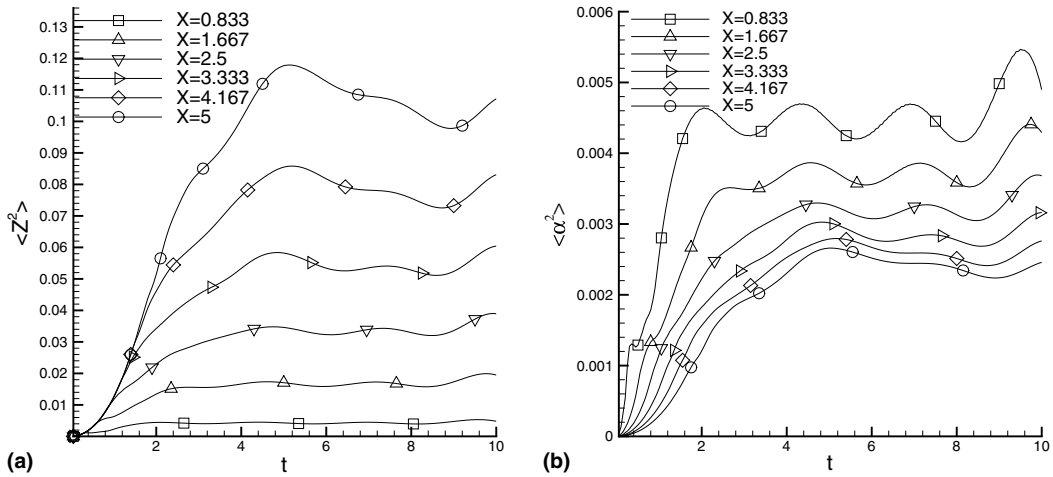
Fig. 8. Variance of (a) the perturbed shock path and (b) of the perturbed shock angle as a function of time t, induced by small random time-dependent wedge motion, described as a random process with correlation length $A = 1$ and amplitude $\epsilon = 0.1$.
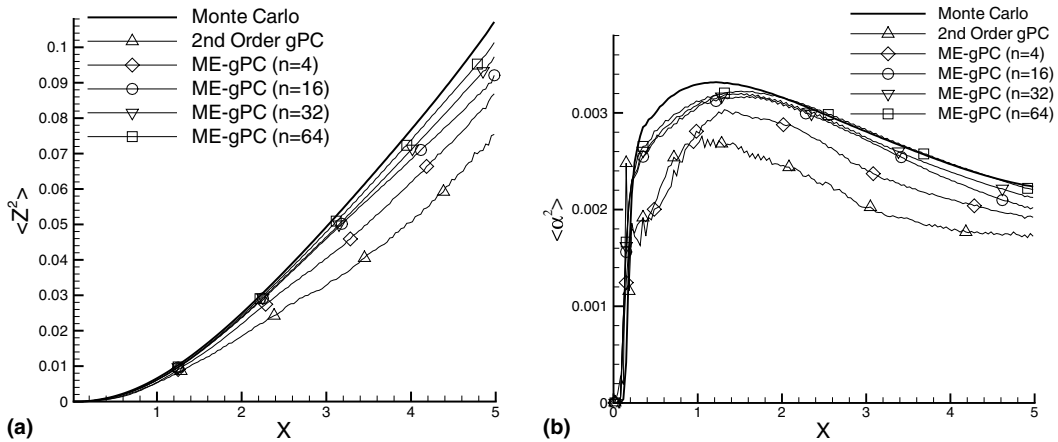
Fig. 9. Variance of (a) the perturbed shock path and (b) of the perturbed shock angle as a function of distance x at $t = 10$, induced by small random time-dependent wedge motion, described as a random process with correlation length $A = 1$ and amplitude $\epsilon = 0.1$.

4.2. Random wedge oscillations

Now, we consider the second case we described earlier where the inflow velocity is deterministic but the wedge undergoes random time-dependent oscillations around its apex. (The results for steady oscillations described as random variable are similar and in good agreement with the analytical solution, see Eq. (14).) We describe this stochastic input as a random process with zero mean and exponential covariance, see Eq. (22). We recall that in the transformed domain, the inflow appears also as a stochastic process as revealed by Eq. (21).

In Fig. 8, we plot the variance of the perturbed shock path and the variance of the perturbed shock angle as a function of time t, induced by small random time-dependent wedge motion, described as a random process with correlation length $A = 1$ and amplitude $\epsilon = 0.1$. In Fig. 9, we plot the same quantities but as a function of distance x from the wedge apex on the wedge surface. We also include the results from Monte-Carlo simulations obtained with 8000 samples. The ME-gPC simulations converge to the Monte-Carlo simulation, as we increase the number of random elements from $N = 4$ to 16, 32 and 64. We also include results from gPC with

second-order which deviate from the Monte-Carlo results, especially for large distances where the variance achieves large values.

5. Summary and discussion

True prediction of the shock dynamics in supersonic flows implies that uncertainties of many types, e.g. due to boundary conditions, geometric regularity, transport coefficients, etc., should be modeled properly and their effect be propagated accurately through the nonlinear flow equations and not simply as an after-thought. This, in turn, implies that we have to reformulate the Euler equations within the stochastic framework thereby expanding the dimensionality of the problem. In addition, we have to revisit classical problems of aerodynamics and formulate semi-analytical solutions and new numerical algorithms for these flow problems. Such efforts represent essential first steps required in setting up solid foundations for stochastic CFD.

The current work on the stochastic wedge flow is a follow-up of our work in [6] on the stochastic piston problem. Here, we have considered two types of randomness associated with inflow conditions and wedge motion, and simulated both as steady as well as time-dependent conditions. For the former case we derived simple analytical solutions, which we used to study the accuracy and convergence properties of the generalized polynomial chaos and its multi-element extension. For time-dependent conditions, modeled as random processes, we resorted to Monte-Carlo simulations for comparisons. Here we have employed Legendre-chaos expansions for uniform random variables but similar algorithms can be constructed for arbitrary probability distributions following the work in [15].

A summary of our findings is as follows: On the physics side, we have shown that the variance of the perturbed-shock location due to the random inflow grows quadratically in space for steady inflow modeled as random variable. However, for time-dependent random inflow perturbations the growth of variance is quadratic at short distances but switches to linear scaling at longer distances. This qualitative spatial transition in the stochastic wedge solution is similar to the temporal transition we have observed for the stochastic piston problem, see [6]. On the numerical side, we have addressed the issue of characteristic flux decomposition within the stochastic framework and have proposed different approaches, including a collocation projection, of the nonlinear terms, in the spirit of pseudo-spectral methods for deterministic problems. Numerical tests have shown that the different flux treatments lead to negligible differences but this may be fortuitous for the current problem. We expect that in viscous supersonic flows with mixed subsonic/supersonic regions the specific characteristic decomposition may play a much more important role. Finally, we note that the multi-element approach is quite effective and more robust than the standard polynomial chaos method. Specifically, we have demonstrated numerically that the convergence of the multi-element generalized polynomial chaos is very fast, with *mean* and *variance* errors decaying as $N^{-2(p+1)}$, where N is the number of random elements and p is the highest order of the polynomial chaos expansion. The multi-element extension reduces errors in long-time integration and produces more accurate results than the global gPC approach at early times. An even more effective approach would be to employ an adaptive scheme following, for example, the magnitude of the variance in each element and refine on-the-fly beyond a certain threshold as it was demonstrated in [14] for simpler problems.

Appendix A

By substituting the gPC expansions for all conservative variables into the two-dimensional transformed Euler equations (19), we obtain the following equations:

$$\sum_{k=0}^{N_p} \frac{\partial}{\partial \tau} \begin{pmatrix} \hat{\rho}_k \phi_k \\ \hat{m}_{r,k} \phi_k \\ \hat{n}_{r,k} \phi_k \\ \hat{E}_{r,k} \phi_k \end{pmatrix} + \sum_{i=0}^{N_p} \frac{\partial}{\partial \zeta} \begin{pmatrix} \hat{m}_{r,i} \phi_i \\ \sum_{j=0}^{N_p} \hat{m}_{r,i} \hat{u}_{r,j} \phi_i \phi_j + \hat{p}_i \phi_i \\ \sum_{j=0}^{N_p} \hat{n}_{r,i} \hat{u}_{r,j} \phi_i \phi_j \\ \sum_{j=0}^{N_p} (\hat{E}_{r,i} + \hat{p}_i) \hat{u}_{r,j} \phi_i \phi_j \end{pmatrix} + \sum_{i=0}^{N_p} \frac{\partial}{\partial \eta} \begin{pmatrix} \hat{n}_{r,i} \phi_i \\ \sum_{j=0}^{N_p} \hat{m}_{r,i} \hat{v}_{r,j} \phi_i \phi_j \\ \sum_{j=0}^{N_p} \hat{n}_{r,i} \hat{v}_{r,j} \phi_i \phi_j + \hat{p}_i \phi_i \\ \sum_{j=0}^{N_p} (\hat{E}_{r,i} + \hat{p}_i) \hat{v}_{r,j} \phi_i \phi_j \end{pmatrix}$$

$$= \sum_{i=0}^{N_p} \begin{pmatrix} 0 \\ -\sum_{j=0}^{N_p} \hat{\rho}_i \cos\theta \frac{\partial \hat{u}_{w,j}}{\partial \tau} \phi_i \phi_j \\ \sum_{j=0}^{N_p} \hat{\rho}_i \sin\theta \frac{\partial \hat{u}_{w,j}}{\partial \tau} \phi_i \phi_j \\ \sum_{j=0}^{N_p} (\hat{n}_{r,i} \sin\theta - \hat{m}_{r,i} \cos\theta) \frac{\partial \hat{u}_{w,i}}{\partial \tau} \phi_i \phi_j \end{pmatrix}. \tag{49}$$

Next we perform a Galerkin projection of the above equations using the same test basis, i.e., ϕ_i and employing the orthogonality relation, we obtain for each $k = 0,\ldots,N_p$:

$$\frac{\partial}{\partial \tau} \begin{pmatrix} \hat{\rho}_k \\ \hat{m}_{r,k} \\ \hat{n}_{r,k} \\ \hat{E}_{r,k} \end{pmatrix} + \frac{\partial}{\partial \zeta} \begin{pmatrix} \hat{m}_{r,k} \\ \frac{1}{\langle \phi_k^2 \rangle} \sum_{i=0}^{N_p} \sum_{j=0}^{N_p} \hat{m}_{r,i} \hat{u}_{r,j} e_{i,j,k} + \hat{p}_k \\ \frac{1}{\langle \phi_k^2 \rangle} \sum_{i=0}^{N_p} \sum_{j=0}^{N_p} \hat{n}_{r,i} \hat{u}_{r,j} e_{i,j,k} \\ \frac{1}{\langle \phi_k^2 \rangle} \sum_{i=0}^{N_p} \sum_{j=0}^{N_p} (\hat{E}_{r,i} + \hat{p}_i) \hat{u}_{r,j} e_{i,j,k} \end{pmatrix} + \frac{\partial}{\partial \eta} \begin{pmatrix} \hat{n}_{rk} \\ \frac{1}{\langle \phi_k^2 \rangle} \sum_{i=0}^{N_p} \sum_{j=0}^{N_p} \hat{m}_{r,i} \hat{v}_{r,j} e_{i,j,k} \\ \frac{1}{\langle \phi_k^2 \rangle} \sum_{i=0}^{N_p} \sum_{j=0}^{N_p} \hat{n}_{r,i} \hat{v}_{r,j} e_{i,j,k} + \hat{p}_k \\ \frac{1}{\langle \phi_k^2 \rangle} \sum_{i=0}^{N_p} \sum_{j=0}^{N_p} (\hat{E}_{r,i} + \hat{p}_i) \hat{v}_{r,j} e_{i,j,k} \end{pmatrix}$$

$$= \begin{pmatrix} 0 \\ -\frac{\epsilon W_1 \cos\theta}{\langle \phi_k^2 \rangle} \sum_{i=0}^{N_p} \sum_{j=1}^{d} \hat{\rho}_i \sqrt{\lambda_j} \frac{\partial f_j}{\partial \tau} e_{i,j,k} \\ \frac{\epsilon W_1 \sin\theta}{\langle \phi_k^2 \rangle} \sum_{i=0}^{N_p} \sum_{j=1}^{d} \hat{\rho}_i \sqrt{\lambda_j} \frac{\partial f_j}{\partial \tau} e_{i,j,k} \\ \frac{\epsilon W_1}{\langle \phi_k^2 \rangle} \sum_{i=0}^{N_p} \sum_{j=1}^{d} (\hat{n}_{r,i} \sin\theta - \hat{m}_{r,i} \cos\theta) \sqrt{\lambda_j} \frac{\partial f_j}{\partial \tau} e_{i,j,k} \end{pmatrix}, \tag{50}$$

where $f_j(\tau)$ and λ_j are the eigenfunctions and eigenvalues of the covariance function and $e_{i,j,k} = \langle \phi_i \phi_j \phi_k \rangle$. Both $\langle \phi_k^2 \rangle$ and $e_{i,j,k}$ can be evaluated analytically during the pre-processing stage. The above system consists of $(N_p + 1)$ deterministic 'Euler-like' equations for each random mode coupled through the convective terms.

Next, we provide details on the equations derived from the ME-gPC treatment. In each element, k, we have

$$\left(-\rho \cos\theta \frac{\partial u_w}{\partial \tau} \right)_k = -\epsilon W_1 \cos\theta \sum_{i=0}^{N_p} \sum_{j=1}^{d} \hat{\rho}_i \phi_i \sqrt{\lambda_j} \frac{\partial f_j}{\partial \tau} \left(\frac{b_{k,j} - a_{k,j}}{2} \xi_{k,j} + \frac{b_{k,j} + a_{k,j}}{2} \right),$$

$$\left(\rho \sin\theta \frac{\partial u_w}{\partial \tau} \right)_k = \epsilon W_1 \sin\theta \sum_{i=0}^{N_p} \sum_{j=1}^{d} \hat{\rho}_i \phi_i \sqrt{\lambda_j} \frac{\partial f_j}{\partial \tau} \left(\frac{b_{k,j} - a_{k,j}}{2} \xi_{k,j} + \frac{b_{k,j} + a_{k,j}}{2} \right),$$

$$\left((n_{r,i}\sin\theta - m_{r,i}\cos\theta)\frac{\partial u_{\mathrm{w}}}{\partial\tau} \right)_k = \epsilon W_1 \sum_{i=0}^{N_p}\sum_{j=1}^{d} (\hat{n}_{r,i}\sin\theta - \hat{m}_{r,i}\cos\theta)\phi_i\sqrt{\lambda_j}\frac{\partial f_j}{\partial\tau}\left(\frac{b_{k,j}-a_{k,j}}{2}\xi_{k,j} + \frac{b_{k,j}+a_{k,j}}{2} \right).$$
(51)

Thus, we can modify Eq. (50) and apply it to each element k to get:

$$
\frac{\partial}{\partial\tau}\begin{pmatrix}\hat{\rho}_k\\ \hat{m}_{r,k}\\ \hat{n}_{r,k}\\ \hat{E}_{r,k}\end{pmatrix}
+ \frac{\partial}{\partial\zeta}\begin{pmatrix}\hat{m}_{r,k}\\ \frac{1}{\langle\phi_k^2\rangle}\sum_{i=0}^{N_p}\sum_{j=0}^{N_p}\hat{m}_{r,i}\hat{u}_{r,j}e_{i,j,k}+\hat{p}_k\\ \frac{1}{\langle\phi_k^2\rangle}\sum_{i=0}^{N_p}\sum_{j=0}^{N_p}\hat{n}_{r,i}\hat{u}_{r,j}e_{i,j,k}\\ \frac{1}{\langle\phi_k^2\rangle}\sum_{i=0}^{N_p}\sum_{j=0}^{N_p}(\hat{E}_{r,i}+\hat{p}_i)\hat{u}_{r,j}e_{i,j,k}\end{pmatrix}
+ \frac{\partial}{\partial\eta}\begin{pmatrix}\hat{n}_{r,k}\\ \frac{1}{\langle\phi_k^2\rangle}\sum_{i=0}^{N_p}\sum_{j=0}^{N_p}\hat{m}_{r,i}\hat{v}_{r,j}e_{i,j,k}\\ \frac{1}{\langle\phi_k^2\rangle}\sum_{i=0}^{N_p}\sum_{j=0}^{N_p}\hat{n}_{r,i}\hat{v}_{r,j}e_{i,j,k}+\hat{p}_k\\ \frac{1}{\langle\phi_k^2\rangle}\sum_{i=0}^{N_p}\sum_{j=0}^{N_p}(\hat{E}_{r,i}+\hat{p}_i)\hat{v}_{r,j}e_{i,j,k}\end{pmatrix}
$$
$$
= \begin{pmatrix}
0\\
-\frac{\epsilon W_1}{\langle\phi_k^2\rangle}\sum_{i=0}^{N_p}\sum_{j=1}^{d}\hat{\rho}_i\cos\theta\sqrt{\lambda_j}\frac{\partial f_j}{\partial\tau}\left(\frac{b_{k,j}-a_{k,j}}{2}e_{i,j,k}+\frac{b_{k,j}+a_{k,j}}{2}e_{i,0,k}\right)\\
\frac{\epsilon W_1}{\langle\phi_k^2\rangle}\sum_{i=0}^{N_p}\sum_{j=1}^{d}\hat{\rho}_i\sin\theta\sqrt{\lambda_j}\frac{\partial f_j}{\partial\tau}\left(\frac{b_{k,j}-a_{k,j}}{2}e_{i,j,k}+\frac{b_{k,j}+a_{k,j}}{2}e_{i,0,k}\right)\\
\frac{\epsilon W_1}{\langle\phi_k^2\rangle}\sum_{i=0}^{N_p}\sum_{j=1}^{d}(\hat{n}_{r,i}\sin\theta-\hat{m}_{r,i}\cos\theta)\sqrt{\lambda_j}\frac{\partial f_j}{\partial\tau}\left(\frac{b_{k,j}-a_{k,j}}{2}e_{i,j,k}+\frac{b_{k,j}+a_{k,j}}{2}e_{i,0,k}\right)
\end{pmatrix}.
$$
(52)

References

[1] S. Schneider, Effects of high-speed tunnel noise on laminar-turbulent transition, J. Spacecraft Rockets 38 (3) (2001) 323–333.

[2] D. Lucor, G.E. Karniadakis, Noisy inflows cause a shedding-mode switching in flow past an oscillating cylinder, Phys. Rev. Lett. 92 (15) (2004) 154501.

[3] C.H.K. Williamson, A. Roshko, Vortex formation in the wake of an oscillating cylinder, J. Fluids Struct. 2 (1988) 355–381.

[4] T. Pottebaum, The relationship between near-wake structure and heat transfer for an oscillating cylinder in cross-flow, Ph.D. Thesis, California Institute of Technology, 2003.

[5] H. Liepmann, A. Roshko, Elements of Gas Dynamics, Wiley, New York, 1957.

[6] G. Lin, C.-H. Su, G.E. Karniadakis, The stochastic piston problem, Proc. Natl. Acad. Sci. USA 101 (45) (2004) 15840–15845.

[7] R.G. Ghanem, P. Spanos, Stochastic Finite Elements: A Spectral Approach, Springer, New York, 1991.

[8] R.G. Ghanem, J. Red-Horse, Propagation of uncertainty in complex physical systems using a stochastic finite elements approach, Physica D 133 (1999) 137–144.

[9] D. Xiu, G.E. Karniadakis, The Wiener–Askey polynomial chaos for stochastic differential equations, SIAM J. Sci. Comput. 24 (2) (2002) 619–644.

[10] D. Xiu, G.E. Karniadakis, Modeling uncertainty in flow simulations via generalized polynomial chaos, J. Comput. Phys. 187 (2003) 137–167.

[11] C. Hirsch, Numerical Computation of Internal and External Flows, Wiley, New York, 1984.

[12] G.-S. Jiang, C.-W. Shu, Efficient implementation of weighted ENO schemes, J. Comput. Phys. 126 (1996) 202–228.

[13] G.E. Karniadakis, S.J. Sherwin, Spectral/hp Element Methods for CFD, second ed., Oxford University Press, Oxford, 2005.

[14] X. Wan, G.E. Karniadakis, An adaptive multi-element generalized polynomial chaos method for stochastic differential equations, J. Comput. Phys. 209 (2005) 617–642.

[15] X. Wan, G.E. Karniadakis, Beyond Wiener–Askey expansions: handling arbitrary PDFs, J. Sci. Comput. (in press).

[16] M.K. Deb, I. Babuška, J.T. Oden, Solution of stochastic partial differential equations using Galerkin finite element techniques, Comput. Meth. Appl. Mech. Eng. 190 (2001) 6359–6372.